Electrostatic Compensation of Structural Imperfections in Dynamically Amplified Dual-Mass Gyroscope

Alexandra Efimovskaya, Yu-Wei Lin, Danmeng Wang, and Andrei M. Shkel
MicroSystems Laboratory, University of California, Irvine, CA 92697, USA
Email: {aefimovs, yuweil4, danmenw, ashkel}@uci.edu

***Abstract*—This paper presents a study on dynamics of a dual-mass MEMS vibratory gyroscope in presence of imperfections and reports a method for precision electrostatic frequency tuning of the operational modes. The presented tuning algorithm involves, first, assessing the modes mismatch using the experimental frequency responses of both proof-masses, followed by the identification of the stiffness mismatch along the two axes and anisoelasticity angles α and β, then choosing the tuning voltages for modification of the diagonal, off-diagonal, and coupling terms in the stiffness matrix. Results of simulation are verified using experimental electrostatic frequency tuning of a dynamically amplified gyroscope. The frequency split between the operational modes was reduced from 26 Hz down to 50 mHz, resulting in 17x increase in the gyroscope scale factor.**

INTRODUCTION

Conceptually, a single-axis gyroscope requires a single proof-mass for measuring the Coriolis acceleration induced angular rate. However, a number of multi-mass solutions have emerged in recent years, pursuing different goals, such as an anchor loss mitigation and a common-mode rejection of shock and vibration [1], improvement of environmental robustness by increasing the bandwidth [2], or dynamic amplification of motion for improved sensitivity [3]-[4].

Along with many advantages of the dual-mass systems, the symmetry of the mode-matched gyroscope with a multi-mass structural element as well as a method for correction of fabrication imperfections is a challenge. Most of the electrostatic tuning methods, previously described in literature, consider a 2-degrees-of-freedom system with a 2x2 stiffness matrix, [5]-[6]. However, increasing a number of proof-masses in gyroscope results in a more complex form of the system stiffness matrix. Hence, new algorithms have to be developed for precision electrostatic tuning.

In this paper, we study the dynamics of an imperfect dual-mass system, using, as an example, a dynamically amplified MEMS gyroscope. A method for electrostatic frequency tuning of such multi-degree of freedom system is described and experimental verification of the proposed approach is presented.

DESIGN AND FABRICATION OF DYNAMICALLY AMPLIFIED GYROSCOPE

We report a design of dynamically amplified gyroscope with a dual-mass architecture (Fig.1), where the increase in structural degrees of freedom is used to improve sensitivity, linearity, and reduce drift. In the amplitude amplified gyroscope, the first, "drive mass", is used for drive and control and the second, "slave mass", is used for sense and is designed to vibrate at amplified amplitude of motion.

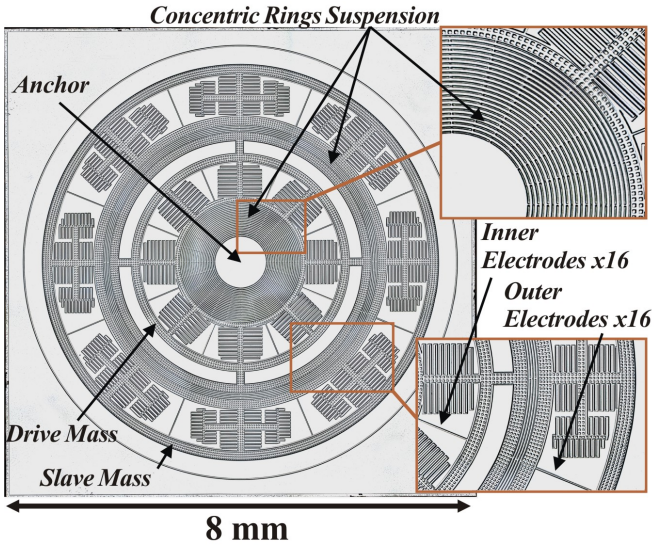

Fig.1. Micro-photograph of fabricated prototype of a dynamically amplified dual-mass gyroscope.

The gyroscope has a footprint of 7.4x7.4 mm^2. It is comprised of an inner, "drive mass", and an outer, "slave mass", mechanically connected by means of the concentric rings suspension. In the rate measuring mode of operation, the drive and sense modes consist of the translational motion of the driving mass and dynamically amplified, in-phase translational motion of the slave mass along the X and Y axes, correspondingly, Fig.2 (a) and (b). In the rate integrating mode of operation, the line of oscillation of two proof-masses precess in presence of Coriolis force, while the motion of the slave mass is dynamically amplified. Devices were designed to operate at the resonant frequency of 17.5 kHz and to provide the dynamic amplification in the range from 5x to 10x.

The suspension is formed by four 18 μm thick concentric rings between the two masses and eleven 18 μm thick concentric rings, connecting the inner mass to the center anchor. Each proof-mass is surrounded by 16 electrodes with parallel plates for drive, pick-off, and electrostatic tuning, Fig.3.

Prototypes of the gyroscope were fabricated using a single-

This material is based on work supported by the Defense Advanced Research Projects Agency and U.S. Navy under Contract No. N66001-16-1-4021.

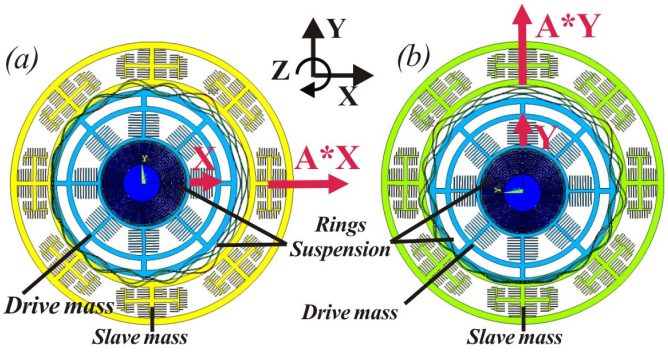

Fig.2. FEA model, showing drive mass motion and amplified motion of slave mass in (a) drive-mode direction; (b) sense-mode direction.

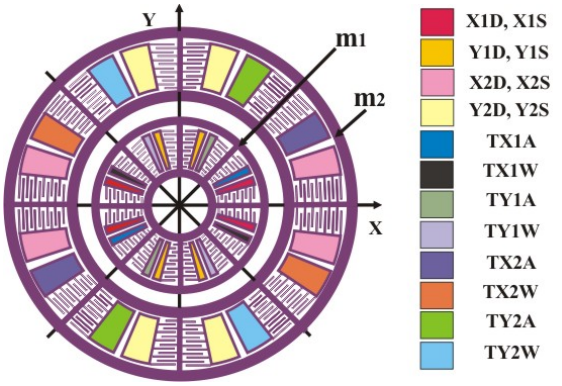

Fig.3. Configuration of driving and tuning electrodes of dynamically amplified dual-mass gyroscope.

mask SOI fabrication process with a 100 μm thick device layer and using a 1.5 μm thick thermal oxide layer as a mask for the deep reactive ion etching of silicon.

Gyroscope Dynamics

The dual-mass gyroscope dynamical system is analyzed in the non-inertial coordinate frame associated with the gyroscope. The equations of motion are derived using a dual mass-spring-damper model. In an "ideal" case, when damping mismatch and structural anisoelasticity are not considered, the governing equations of motion of a gyroscope, measuring rotation about the z-axis, are expressed in matrix form as

$$[M]\ddot{q} + [C]\dot{q} + [K]q + [R_c]\dot{q} = [F], \tag{1}$$

where q is the vector of the generalized coordinates $q = [x_1 y_1 x_2 y_2]^T$. The generalized mass and damping matrices have the structure:

$$M = \begin{bmatrix} m_1 & 0 & 0 & 0 \\ 0 & m_1 & 0 & 0 \\ 0 & 0 & m_2 & 0 \\ 0 & 0 & 0 & m_2 \end{bmatrix}, C = \begin{bmatrix} c_1 & 0 & 0 & 0 \\ 0 & c_1 & 0 & 0 \\ 0 & 0 & c_2 & 0 \\ 0 & 0 & 0 & c_2 \end{bmatrix}$$

The external force vector and the Coriolis force matrix have the structure:

$$F = \begin{bmatrix} F_{x1} \\ F_{y1} \\ 0 \\ 0 \end{bmatrix}, R_c = \begin{bmatrix} 0 & -2m_1\Omega & 0 & 0 \\ 2m_1\Omega & 0 & 0 & 0 \\ 0 & 0 & 0 & -2m_2\Omega \\ 0 & 0 & 2m_2\Omega & 0, \end{bmatrix}$$

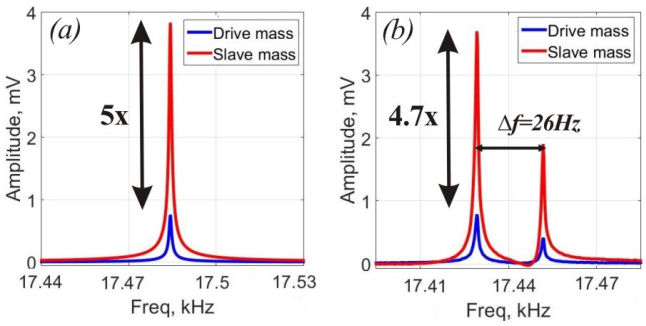

Fig.4. (a) Simulated freq. response with predicted amplification of 5x. (b) Experimental response with coupling of drive and sense modes: Δf=26Hz; amplification 4.7x.

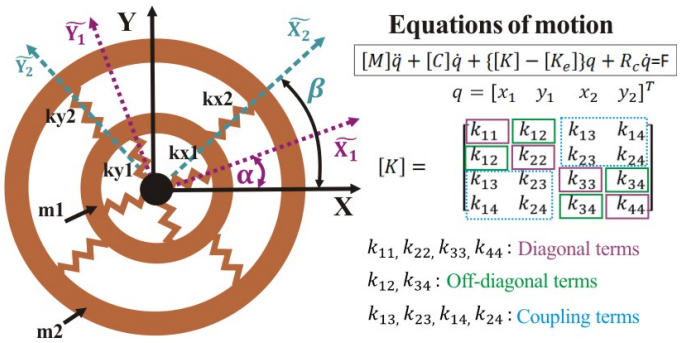

Fig.5. Imperfections in suspension and mass cause the misalignment of principle axes of elasticity. Anisoelasticity angles for inner and outer masses are denoted as α and β.

where Ω is the angular rate applied around the Z axis.

Finally, the generalized stiffness matrix has the structure:

$$K = \begin{bmatrix} k_{x1} + k_{x2} & 0 & -k_{x2} & 0 \\ 0 & k_{y1} + k_{y2} & 0 & -k_{y2} \\ -k_{x2} & 0 & k_{x2} & 0 \\ 0 & -k_{y2} & 0 & k_{y2} \end{bmatrix}, \tag{2}$$

where k_{x1} and k_{x2} are the stiffness coefficients along the X axis for the inner and the outer mass suspension, correspondingly; k_{y1} and k_{y2} are the stiffness coefficients along the Y axis for the inner and the outer mass suspension, correspondingly, Fig.5.

Experimental Frequency Response

Experimental frequency response of the sensor was obtained using electrostatic excitation with 10V DC voltage and 60mV AC voltage applied to the X1D driving electrodes of the inner mass. Characterization of the fabricated prototype revealed the central frequency of 17.44 kHz with the amplification factor of 4.7x and the frequency split (Δf) of 26 Hz, Fig.4(b).

The first peak on the sense-mode frequency response curve in Fig.4(b) corresponds to the frequency of the sense mode, the second peak corresponds to the frequency of the drive mode and is caused by the coupling of the drive motion to the sense mode. This coupling leads to the energy distribution

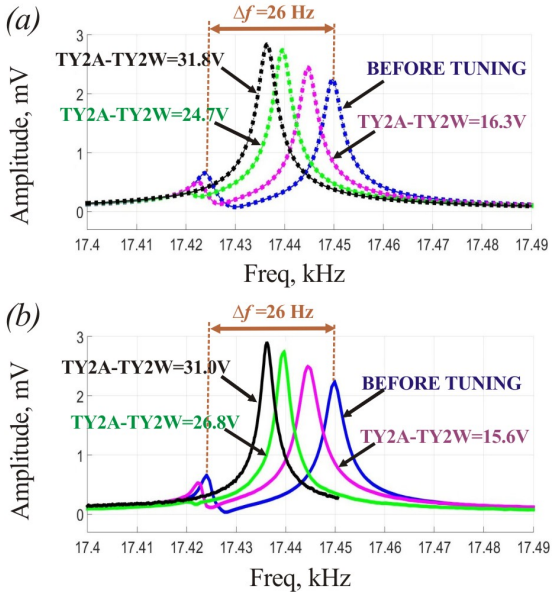

Fig.6. Freq. response showing tuning of the off-diagonal terms of stiffness matrix and reduction of coupling between modes: (a) simulated; (b) experimental.

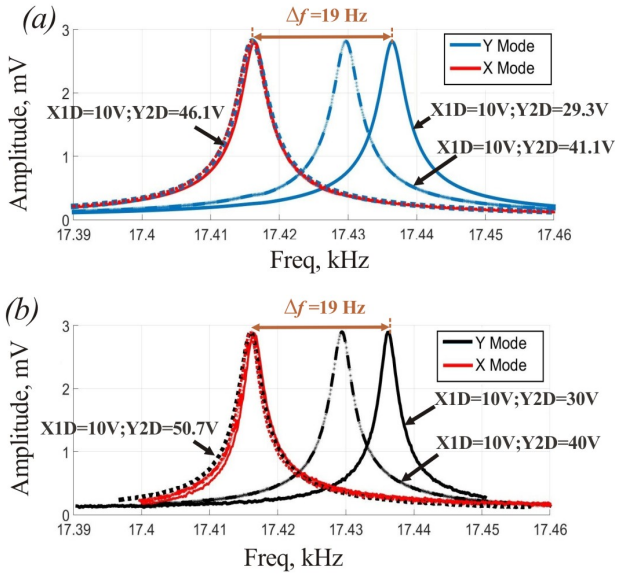

Fig.7. Freq. response showing tuning of the diagonal terms of stiffness matrix and reduction of frequency split between modes: (a) simulated; (b) experimental.

between the modes and results in reduced amplitude amplification factor as compared to the analytically predicted, 4.7x vs 5x, Fig.4.

Electrostatic Correction of Structural Imperfections

Experimental frequency characterization of 12 prototypes revealed a frequency split between the modes (Δf) in the range from 25 Hz to 59 Hz, which arises from fabrication-induced asymmetries in mechanical element. In case of a dual-mass gyroscope, the structural symmetry is defined by a 4x4 stiffness matrix (2).

Imperfections in suspension and mass cause the misalignment of the principle axes of elasticity [7]-[8] of both masses, resulting in non-zero off-diagonal terms of the stiffness matrix and increased coupling between the drive and sense modes, Fig. 5. Fabrication imperfections of both masses also result in non-equal diagonal terms of the stiffness matrix, leading to frequency splits between the modes.

The resulting generalized stiffness matrix for the dual-mass system in presence of stiffness imperfections has the structure:

$$K = \begin{bmatrix} k_{11} & k_{12} & k_{13} & k_{14} \\ k_{12} & k_{22} & k_{23} & k_{24} \\ k_{13} & k_{23} & k_{33} & k_{34} \\ k_{14} & k_{24} & k_{34} & k_{44} \end{bmatrix}, \tag{3}$$

where

$$\begin{aligned} k_{11} &= cos^2\alpha(k_{x1}+k_{x2}) + sin^2\alpha(k_{y1}+k_{y2}); \\ k_{12} &= 0.5 * sin2\alpha(k_{x1}+k_{x2}-k_{y1}-k_{y2}); \\ k_{13} &= -k_{x2}cos\beta * cos\alpha - k_{y2}sin\beta * sin\alpha; \\ k_{14} &= -k_{x2}sin\beta * cos\alpha + k_{y2}cos\beta * sin\alpha; \\ k_{22} &= sin^2\alpha(k_{x1}+k_{x2}) + cos^2\alpha(k_{y1}+k_{y2}); \\ k_{23} &= -k_{x2}cos\beta * sin\alpha + k_{y2}sin\beta * cos\alpha; \\ k_{24} &= -k_{x2}sin\beta * sin\alpha - k_{y2}cos\beta * cos\alpha; \\ k_{33} &= cos^2\beta * k_{x2} + sin^2\beta * k_{y2}; \\ k_{34} &= 0.5 * sin2\beta(k_{x2}-k_{y2}); \\ k_{44} &= sin^2\beta * k_{x2} + cos^2\beta * k_{y2}. \end{aligned}$$

Here, α and β are the anisoelasticity angles for the inner and outer mass, correspondingly.

Our method for precision electrostatic frequency tuning of the operational modes is based on estimation of the anisoelasticity angles using the experimental frequency responses of inner and outer proof-masses, followed by identification of the tuning voltages using an analytical solution of the dynamic equations in presence of imperfections:

$$[M]\ddot{q} + [C]\dot{q} + ([K] - [K_e])q + [R_c]\dot{q} = [F], \tag{4}$$

where $([K] - [K_e])$ is the electrostatically modified stiffness matrix.

Electrostatic tuning matrix has the structure:

$$K_e = \begin{bmatrix} k_{e11} & k_{e12} & 0 & 0 \\ k_{e12} & k_{e22} & 0 & 0 \\ 0 & 0 & k_{e33} & k_{e34} \\ 0 & 0 & k_{e34} & k_{e44} \end{bmatrix}. \tag{5}$$

The experimental frequency responses of the drive and slave masses were fitted to the analytical solutions of the dynamic equations (1) for the dual-mass system in presence of imperfections. For the prototype of the dynamically amplified gyroscope with a 26 Hz frequency split (Δf) between the operation mode, the anisoelasticity angles α= 29° and β=26° were found.

Next, the terms of the matrix K_E for tuning the diagonal, off-diagonal and coupling terms were analytically identified

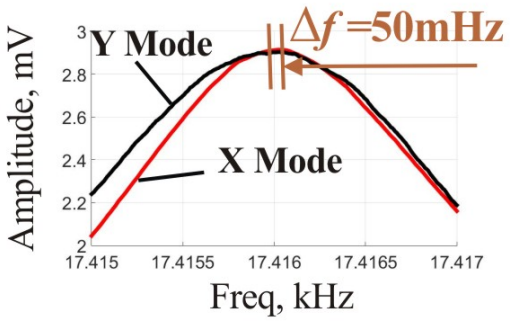

Fig.8. Using simultaneous tuning of diagonal, off-diagonal, and coupling terms in stiffness matrix, the frequency split between the operational modes was reduced from 26 Hz down to 50 mHz.

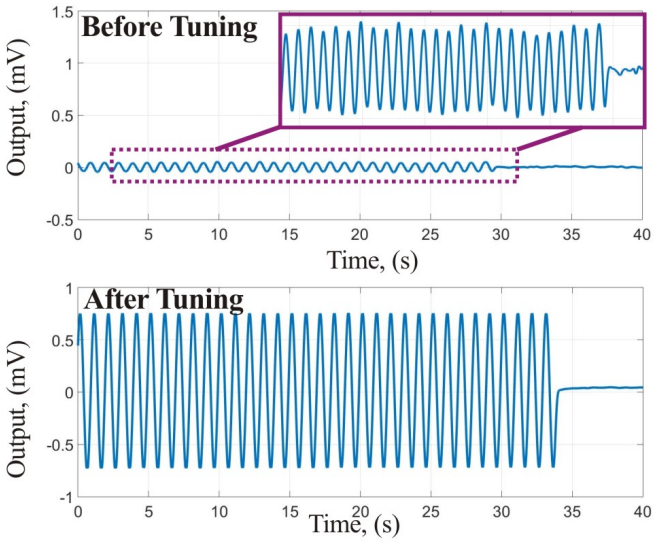

Fig.9. Gyroscope response to sinusoidal input of the rate table, showing 17x higher SF and stable amplitude after tuning.

and the necessary tuning voltages for the two masses were determined.

The DC voltages were applied to the electrodes (TY2A, TY2W) and (TY1A, TY1W) to modify the off-diagonal terms of the stiffness matrix, Fig.6 (b). To compensate for the coupling between the modes, the DC voltage of 31 V was applied between the electrodes (TY2A, TY2W), while the DC voltage of 24.7 V was applied between the electrodes (Y1A, TY1W). This result is in good agreement with the analytically predicted values, Fig.6 (a).

In addition, the DC voltage of 50.7 V was applied to the electrodes Y2D to modify the diagonal terms of the stiffness matrix, enabling mode matching, Fig.7 (b). The predicted value of the DC voltage to be applied to these pair of electrodes was 46.1 V, which is in good agreement with the experiment, Fig.7 (a).

The coupling terms of the stiffness matrix, arising from the mechanical coupling of the two masses, are compensated during the simultaneous off-diagonal tuning and diagonal tuning.

During the higher precision tuning, when the resonant peaks of the gyroscope were tracked in the narrow range of frequencies, operational modes were tuned down to 50 mHz using the following DC voltages: TY2A-TY2W=29.6V; TY1A-TY1W=24.7V; Y2D=50.7V, Fig.8. Lower tuning voltages can be used if the Y2S electrodes in addition to the Y2D electrodes are assigned for the diagonal tuning.

The rate table characterization of the gyroscope before and after tuning showed an increase in scale factor by more than an order of magnitude, from 0.0045 mV/deg/s to 0.0766 mV/deg/s, Fig.9.

Conclusion

An analytical model of a dual-mass system in presence of imperfections has been presented and a method of electrostatic compensation of structural imperfections in dual-mass gyroscope has been reported. The tuning procedure is based on estimation of the modes mismatch and coupling between the modes, utilizing the experimental frequency response data. The analytical model is then used to determine the necessary tuning voltages to permit the removal of anisoelasticity and the principle axes stiffness mismatch, thus enabling the gyroscope operational modes to be tuned.

The method of electrostatic tuning was validated through the experimental characterization of a dual-mass dynamically amplified gyroscope, where the frequency split between the operational modes was reduced from 26 Hz down to 50 mHz, resulting in 17x increase in the gyroscope scale factor.

Acknowledgment

Design, fabrication, and characterization were performed in UCI Microsystems Laboratory. Devices were fabricated at UCI INRF facility.

References

[1] D. Senkal, A. Efimovskaya, A. M. Shkel, *Dual Foucault Pendulum gyroscope*, IEEE Transducers 2015 Conference 2015, Alaska, USA, June 21-25, (2015).

[2] C. Acar and A. M. Shkel, *Inherently Robust Micromachined Gyroscopes With 2-DOF Sense-Mode Oscillator*, IEEE Journal of Microelectromechanical Systems, Vol. 15, No. 2, pp. 380-387, (2006).

[3] C. Painter, A. M Shkel, *Dynamically Amplified Rate Integrating Gyroscopes*, U.S. Patent 6,928,874, (2005).

[4] C. Painter, A. M Shkel, *Dynamically Amplified Rate Integrating Gyroscopes*, Proc. NSTI Nanotechnology Conference and Trade Show Nanotech 2003, San Francisco CA, USA, February 23-27, (2003).

[5] Z.X. Hu, B. J. Gallacher, J.S. Burdess, S.R. Bowles and H.T.D. Grigg, *A systematic approach for precision electrostatic mode tuning of a MEMS gyroscope*, IOP Journal of Micromechanics and Microengineering, Vol. 24, No. 12, (2014).

[6] B.J. Gallacher, J. Hedley, J.S. Burdess, A.J. Harris, A. Rickard, and D.O. King, *Electrostatic Correction of Structural Imperfections Present in a Microring Gyroscope*, IEEE Journal of Microelectromechanical Systems, Vol. 14, No. 2, pp. 221-234, (2005).

[7] C. Painter and A. Shkel, *Identification of anisoelasticity for electrostatic trimming of rate integrating gyroscopes*, Proc. 2002 SPIE Annual International Symposium on Smart Structures and Materials, San Diego, CA, March 17, (2002).

[8] A.S. Phani, and A. A. Seshia, *Identification of Anisoelasticity and Non-proportional Damping in MEMS Gyroscopes*, Proc. NSTI Nanotechnology Conference and Trade Show Nanotech 2004, Boston, Massachusetts, USA, March 7-11, (2004).